We are IntechOpen, the world's leading publisher of Open Access books Built by scientists, for scientists

4,800
Open access books available

122,000
International authors and editors

135M
Downloads

Our authors are among the

154
Countries delivered to

TOP 1%
most cited scientists

12.2%
Contributors from top 500 universities

CLARIVATE ANALYTICS BOOK CITATION INDEX INDEXED

WEB OF SCIENCE™

Selection of our books indexed in the Book Citation Index in Web of Science™ Core Collection (BKCI)

Interested in publishing with us?
Contact book.department@intechopen.com

Numbers displayed above are based on latest data collected.
For more information visit www.intechopen.com

Chapter 3

Full-Wave Spectral Analysis of Resonant Characteristics and Radiation Patterns of High Tc Superconducting Circular and Annular Ring Microstrip Antennas

Ouarda Barkat

Additional information is available at the end of the chapter

http://dx.doi.org/10.5772/54665

1. Introduction

During the last decades, superconducting antenna was one of the first microwave components to be demonstrated as an application of high-temperature superconducting material [1-3]. High *Tc* superconducting microstrip antennas (HTSMA) are becoming popular and getting increased attention in both theoretical research and engineering applications due to their excellent advantages. Various patch configurations implemented on different types of substrates have been tested and investigated. In the design of microstrip antennas, anisotropic substances have been increasingly popular. Especially the effects of uniaxial type anisotropy have been investigated due to availability of this type of substances. These structures characterized by their low profile, small size, light weight, low cost and ease of fabrication, which makes them very suitable for microwave and millimeter-wave device applications [4-6]. HTSMA structures have shown significant superiority over corresponding devices fabricated with normal conductors such as gold, silver, or copper. Major property of superconductor is very low surface resistance; this property facilitates the development of microstrip antennas with better performance than conventional antennas. Compared to other patch geometries, the circular and annular ring microstrip patches printed on a uniaxial anisotropic substrate, have been more extensively studied for a long time by a number of investigators [7-11]. Circular microstrip patch can be used either as radiating antennas or as oscillators and filters in microwave integrated circuits (MIC's). The inherent advantage of an annular ring antenna is: first, the size of an annular ring for a given mode of operation is smaller than that of the circular disc resonating at the same frequency. Second, The presence of edges at the inner and outer radii causes more fringing than in the case of a circular microstrip antenna, in which fringing occurs only at the outer edge, and this implies more radiation from these edges, that leads to

high radiation efficiency. These structures are quite a complicated structure to analyze mathematically. Different models are available to model a microstrip antenna as the transmission-line model and the cavity model in simple computer aided design formulas. However, the accuracy of these approximate models is limited, and only suitable for analysing simple regularly shaped antenna or thin substrates. The full-wave spectral domain technique is extensively used in microstrip antennas analysis and design. In this method, Galerkin's method, together with Parsval's relation in Hankel transform domain is then applied to compute the resonant frequency and bandwidth. The integral equation is formulated with Hankel transforms which gives rise to a diagonal form of the Green's function in spectral domain.

The numerical results for the resonant frequency, bandwidth and radiation pattern of microstrip antennas with respect to anisotropy ratio of the substrate, are presented. The Influence of a uniaxial substrate on the radiation of structure has been studied. To include the effect of the superconductivity of the microstrip patch in the full wave spectral analysis, the surface complex impedance has been considered. The effect of the temperature and thickness of HTS thin film on the resonant frequency and bandwidth have been presented. Computations show that, the radiation pattern of the antenna do not vary significantly with the permittivity variation perpendicular to the optical axis. Moreover, it is found to be strongly dependent with the permittivity variation along the optical axis. The computed data are found to be in good agreement with results obtained using other methods. Also, the TM and TE waves are naturally separated in the Green's function. The stationary phase method is used for computing the far-zone radiation patterns.

2. Theory

The antenna configurations of proposed structures are shown in Figure 1. The superconducting patches are assumed to be located on grounded dielectric slabs of infinite extent, and the ground planes are assumed to be perfect electric conductors. The substrates of thickness d are considered to be a uniaxial medium with permittivity tensor:

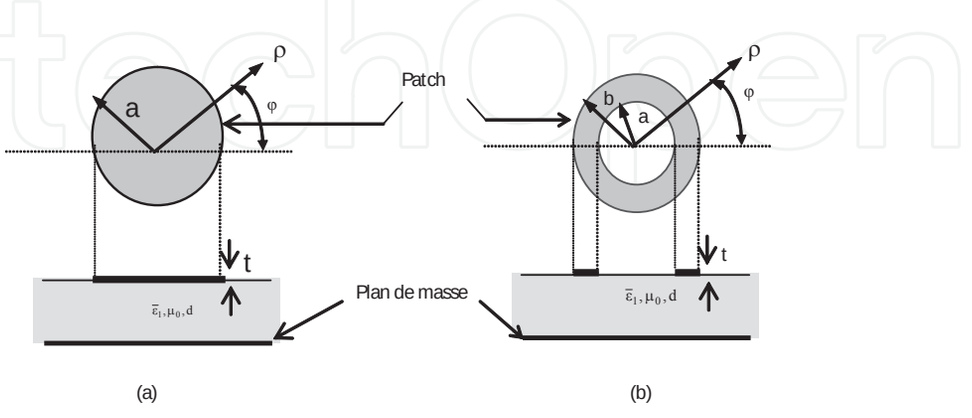

Figure 1. Cross section of a superconducting microstrip patch on uniaxial anisotropic media. (a) circulaire ; (b) annulaire ring

http://dx.doi.org/10.5772/54665

$$\bar{\bar{\varepsilon}}_j = \varepsilon_0 \begin{vmatrix} \varepsilon_{jx} & 0 & 0 \\ 0 & \varepsilon_{jy} & 0 \\ 0 & 0 & \varepsilon_{jz} \end{vmatrix} \tag{1}$$

Where $\varepsilon_{jx} = \varepsilon_{jy} \neq \varepsilon_{jz}$ (j=1, 2), and the permeability will be taken as μ_0.

Starting from Maxwell's equations in the Hankel transform domain, we can show that the transverse fields inside the uniaxial anisotropic region can be written as [12]:

$$\mathbf{E}_\rho(\rho,\phi,z_j) = \sum_{n=-\infty}^{\infty} e^{in\varphi} \int_0^{\infty} dk_\rho k_\rho \; [\frac{\omega\mu_0}{2k_\rho}(\tilde{J}_{n-1}(k_\rho\rho) + \tilde{J}_{n+1}(k_\rho\rho)) \cdot \tilde{\mathbf{H}}_{\mathbf{jz}}\left(k_\rho, z_j\right) + \frac{i\varepsilon_{jz}}{2k_\rho\varepsilon_{jx}}(-\tilde{J}_{n+1}(k_\rho\rho) + \tilde{J}_{n-1}(k_\rho\rho))\frac{\partial\, \tilde{\mathbf{E}}_{\mathbf{jz}}\left(k_\rho, z_j\right)}{\partial\, \mathbf{z}}] \tag{2}$$

$$\mathbf{E}_\phi(\rho,\phi,z_j) = \sum_{n=-\infty}^{\infty} e^{in\varphi} \int_0^{\infty} dk_\rho k_\rho \; [i\frac{\omega\mu_0}{2\,k_\rho}(\tilde{J}_{n-1}(k_\rho\rho) - \tilde{J}_{n+1}(k_\rho\rho)) \cdot \tilde{\mathbf{H}}_{\mathbf{jz}}\left(k_\rho, z_j\right) - \frac{\varepsilon_{jz}}{2\varepsilon_{jx}k_\rho}(\tilde{J}_{n+1}(k_\rho\rho) + \tilde{J}_{n-1}(k_\rho\rho))\frac{\partial\, \tilde{\mathbf{E}}_{\mathbf{jz}}\left(k_\rho, z_j\right)}{\partial\, \mathbf{z}}] \tag{3}$$

$$\mathbf{H}_\varphi(\rho,\phi,z_j) = \sum_{n=-\infty}^{\infty} e^{in\varphi} \int_0^{\infty} dk_\rho k_\rho \; [(\frac{\dot{\omega}\,\varepsilon_{jz}\varepsilon_0}{2k_\rho}\left(\tilde{J}_{n-1}(k_\rho\rho) - \tilde{J}_{n+1}(k_\rho\rho)\right)\cdot \tilde{\mathbf{E}}_{\mathbf{jz}}\left(k_\rho, z_j\right) + \frac{1}{2k_\rho}(\tilde{J}_{n-1}(k_\rho\rho) + \tilde{J}_{n+1}(k_\rho\rho))\cdot\frac{\partial\, \tilde{\mathbf{H}}_{\mathbf{jz}}\left(k_\rho, z_j\right)}{\partial\, \mathbf{z}}] \tag{4}$$

$$\mathbf{H}_\rho(\rho,\phi,z_j) = \sum_{n=-\infty}^{\infty} e^{in\varphi} \int_0^{\infty} dk_\rho k_\rho \; [\frac{\omega\varepsilon_{jz}\varepsilon_0}{2k_\rho}(\tilde{J}_{n-1}(k_\rho\rho) + \tilde{J}_{n+1}(k_\rho\rho))\cdot \tilde{\mathbf{E}}_{\mathbf{jz}}\left(k_\rho, z_j\right) + \frac{\mathrm{i}}{2k_\rho}(\tilde{J}_{n+1}(k_\rho\rho) - \tilde{J}_{n-1}(k_\rho\rho))\frac{\partial\, \tilde{\mathbf{H}}_{\mathbf{jz}}\left(k_\rho, z_j\right)}{\partial\, \mathbf{z}}] \tag{5}$$

We can put these equations in the following form:

$$\mathbf{E}(\rho,\phi,z_j) = \begin{bmatrix} \mathbf{E}_\rho(\rho,\phi,z_j) \\ \mathbf{E}_\phi(\rho,\phi,z_j) \end{bmatrix} = \sum_{n=-\infty}^{+\infty} e^{jn\phi} \int_0^{+\infty} dk_\rho .\; k_\rho . \bar{\mathbf{H}}_{\mathbf{n}}(k_\rho\rho). \begin{bmatrix} (i\varepsilon_{jz}/\varepsilon_{jx}).\partial\, \tilde{\mathbf{E}}_{\mathbf{jz}}(k_\rho, z_j)/\partial\, \mathbf{z} \\ \dot{\omega}\,\mu_{\rho}\tilde{\mathbf{H}}_{\mathbf{jz}}\left(k\;, z_j\right) \end{bmatrix} \tag{6}$$

$$H(\rho,\phi,z_j) = \begin{bmatrix} \mathbf{H}_\phi(\rho,\phi,z_j) \\ -\mathbf{H}_\rho(\rho,\phi,z_j) \end{bmatrix} = \sum_{n=-\infty}^{+\infty} e^{jn\phi} \int_0^{+\infty} dk_\rho .k_\rho . \bar{\mathbf{H}}_{\mathbf{n}}(k_\rho\rho). \begin{bmatrix} \dot{\omega}\;\varepsilon_{\mathbf{jz}}\varepsilon_0\;\tilde{\mathbf{E}}_{\mathbf{jz}}(k\;, z_j) \\ i\partial\;\tilde{\mathbf{H}}_{\mathbf{jz}}(k_\rho, z_j)/\partial\;\mathbf{z} \end{bmatrix} \tag{7}$$

That is

$$H(\rho,\phi,z_j) = \sum_{n=-\infty}^{+\infty} e^{jn\phi} \int_0^{+\infty} dk_\rho .k_\rho . \bar{\mathbf{H}}_{\mathbf{n}}(k_\rho\rho).\tilde{e}_n(k_\rho, z) \tag{8}$$

$$\mathbf{E}(\rho,\phi,z_j) = \sum_{n=-\infty}^{+\infty} e^{jn\phi} \int_0^{+\infty} dk_\rho .k_\rho . \bar{\mathbf{H}}_{\mathbf{n}}(k_\rho\rho).\tilde{h}_n(k_\rho, z) \tag{9}$$

The kernel of the vector Hankel transform is given by [12]:

$$\overline{H}_n(k_\rho\rho)=\begin{vmatrix} \dot{J}_n(k_\rho\rho) & -in\,J_n(k_\rho\rho)/k_\rho \\ in\,J_n(k_\rho\rho)/k_\rho\rho & \dot{J}_n(k_\rho\rho) \end{vmatrix} \tag{10}$$

And

$$\tilde{e}_n(k_\rho,z)=\bar{\mathbf{A}}_{nj}\left(k_\rho\right)e^{-i\,\bar{k}_{jz}z}+\bar{\mathbf{B}}_{nj}\left(k_\rho\right)e^{i\,\bar{k}_{jz}z} \tag{11}$$

$$\tilde{h}_n(k_\rho,z)=\bar{\mathbf{g}}_j\,(\mathrm{k}_\rho).(\bar{\mathbf{A}}_{nj}\left(k_\rho\right)e^{-i\,\bar{k}_{jz}z}-\bar{\mathbf{B}}_{nj}\left(k_\rho\right)e^{i\,\bar{k}_{jz}z} \tag{12}$$

$\bar{A}$ and $\bar{B}$ are two unknown vectors and $\bar{g}(k_\rho)$ is determined by:

$$\bar{g}_j(k_\rho)=\begin{vmatrix} \omega\varepsilon_{jx}\varepsilon_0/k_{jz}^h & 0 \\ 0 & k_{jz}^e/\omega\mu_0 \end{vmatrix} \tag{13}$$

Where

k_0 : is the free space wavenumber,

$k_{jz}^e=(\varepsilon_{jx}k_0^2-(\varepsilon_{jx}k_\rho^2/\varepsilon_{jz}))^{1/2}$: is TM propagation constants in the uniaxial substrate.

$k_{jz}^h=(\varepsilon_{jx}k_0^2-k_\rho^2)^{\frac{1}{2}}$: is TE propagation constants in the uniaxial substrate.

In the spectral domain, the relationship between the patch current and the electric field on the microstrip is given by [10, 11]:

$$\tilde{\mathbf{E}}\left(\mathbf{k}_\rho\right)=\bar{\mathbf{G}}\left(\mathbf{k}_\rho\right).\tilde{K}\left(\mathbf{k}_\rho\right) \tag{14}$$

$\tilde{K}(\boldsymbol{k}_\rho)$is the current on the microstrip which related to the vector Hankel transform of K(ϱ). The unknown currents are expanded, in terms of a complete orthogonal set of basis functions, issued from the magnetic wall cavity model. It is possible to find a complete set of vector basis functions to approximate the current distribution, by noting that the superposition of the currents due to TM and TE modes of a magnetic-wall cavity form a complete set. The current distribution of the nth mode of microstrip patch can be written as [11, 12]:

$$K_n\left(\rho\right)=\sum_{p=1}^{P}a_{np}\boldsymbol{\Psi}_{np}\left(\rho\right)+\sum_{q=1}^{Q}b_{nq}\boldsymbol{\Phi}_{nq}\left(\rho\right) \tag{15}$$

http://dx.doi.org/10.5772/54665

Here a_{np} and b_{nq} are unknown coefficients.

For superconducting annular ring patch, (α_{nq}, β_{np}) are the roots of dual equations $\varphi_n(\alpha_{nq}b/a)=0$ and $\psi_n'(\beta_{np}b/a)=0$.

The Hankel transforms of ψ_{np} and φ_{nq} functions are described as [12]:

$$\tilde{\Psi}_{np}\left(k_\rho\right)=\begin{cases}\left[\dfrac{\beta_{np}/a)}{((\beta_{np}/a)^2-k_\rho^2)}Y'_{np}(k_\rho)\right]\rho & a<\rho<b\\ \left[\dfrac{na}{\beta_{np}k_\rho)}Y_{np}(k_\rho)\right]\rho & \\ 0 & \rho>b,\quad \rho<a\end{cases} \tag{16}$$

$$\tilde{\Phi}_{nq}\left(k_\rho\right)=\begin{cases}\left[\begin{array}{c}0\\ \dfrac{k_\rho a}{(k_\rho^2-(\alpha_{nq}/a)^2)}Z_{nq}(k_\rho)\end{array}\right]\rho & a<\rho<b\\ 0 & \rho>b,\quad \rho<a\end{cases} \tag{17}$$

Where

$$Y_{pp}\left(k\right)=\psi_n(\beta_{np}b/a)J_n(k\,b)-\psi_n(\beta_{np})J_n(k\,a) \tag{18}$$

$$Z_{pq}\left(k\right)=(b/a)\;\;'_n(\;\;b)J_n(k\,b)-\;\;'_n(\;\;)J_n(k\,a) \tag{19}$$

Using the same procedure, the basis functions for superconducting circular patch, are given by the expressions [11]:

$$\tilde{\Psi}_{np}(k_\rho)=\beta_{np}aJ_n(\beta_{np}a)\left[\frac{\dot{J}_n(k_\rho a)}{\beta_{np}^2-k_\rho^2}\quad\frac{in}{k_\rho\beta_{np}^2a}J_n(k_\rho a)\right]^T \tag{20}$$

$$\tilde{\varphi}_{nq}(k_\rho)=\left[0\quad\frac{k_\rho a\dot{J}_n(\alpha_{nq}a)J_n(k_\rho a)}{k_\rho^2-\alpha_{nq}^2}\right]^T \tag{21}$$

Where

$\dot{J}_n(\beta_{np}a)=0$ and $J_n(\alpha_{nq}a)=0$.

$J_n(.)$ and $N_n(.)$ are the Bessel functions of the first, and second kind of order n.

$\overline{G}(k_\rho)$ is the spectral dyadic Green's function, and after some simple algebraic manipulation, we determine the closed form of the spectral Green dyadic at z=d for a grounded uniaxial substrate.

$$\overline{G} = \begin{bmatrix} G^{TM} & 0 \\ 0 & G^{TE} \end{bmatrix} \tag{22}$$

Where

$$G^{TM} = \frac{k_0}{i\omega\ \varepsilon_0}\frac{k_z^e.\sin(k_z^e d)}{\varepsilon_x.k_0.\cos(k_z^e d) + ik_z^e.\sin(k_z^e d)} \tag{23}$$

$$G^{TE} = \frac{k_0^2}{i\omega\ \varepsilon_0}.\frac{\sin(k_z^h d)}{k_z^h \cos(k_z^h d) + ik_0 \sin(k_z^h d)} \tag{24}$$

In order to incorporate the finite thickness, the dyadic Green's function is modified by considering a complex boundary condition. The surface impedance of a high-temperature superconductors (HTSs) material for a plane electromagnetic wave incident normally to its surface is defined as the ratio of |E| to |H| on the surface of the sample [13]. It is described by the equation:

$$Z_s = R_s + i\ X_s \tag{25}$$

Where R_s and X_s are the surface resistance and the surface reactance.

If the thickness t of the strip of finite conductivity σ is greater than three or four penetration depths, the surface impedance is adequately represented by the real part of the wave impedance [13].

$$Z_s = \sqrt{\omega\mu_0 / (2.\sigma)} \tag{26}$$

If t is less than three penetration depths, a better boundary condition is given by [13]:

$$Z_s = 1/t\sigma \tag{27}$$

Where the conductivity $\sigma = \sigma_c$ is real for conventional conductors. These approximations have been verified for practical metallization thicknesses by comparison with rigorous mode matching result.

http://dx.doi.org/10.5772/54665

For superconductors, a complex conductivity of the form $\sigma = \sigma_n (T/T_c)^4 - i(1-(T/T_c)^4)/\omega\mu_0\lambda_0^2$, where σ_n is often associated with the normal state conductivity at T_c and λ_0 is the effective field penetration depth.

Now, we have the necessary Green's function, it is relatively straightforward to formulate the moment method solution for the antenna characteristics. The boundary condition at the surface of the microstrip patch is given by:

$$\bar{\mathbf{E}}_{scat} + \bar{\mathbf{E}}_{inc} - \bar{Z}_{\mathbf{s}} \cdot \bar{K}_n = 0 \tag{28}$$

Here $\bar{\boldsymbol{E}}_{inc}$ and $\bar{\boldsymbol{E}}_{scat}$ are tangential components of incident and scattered electrics fields. Electric field is enforced to satisfy the impedance boundary condition on the microstrip patch, and the current vanishes off the microstrip patch, to give the following set of vector dual integral equations [3]. For superconducting annular ring microstrip antenna, we have:

$$e_n(\rho) = \int_0^\infty dk_\rho k_\rho \bar{H}_n(k_\rho\rho) \cdot (\bar{G}(k_\rho) - \bar{Z}_S)\bar{K}_n(k_\rho) = \mathbf{0} \qquad a < \rho < b \tag{29}$$

$$K_n(\rho) = \int_0^\infty dk_\rho k_\rho \bar{H}_n(k_\rho\rho) \cdot \bar{K}_n(k_\rho) = \mathbf{0} \qquad \rho > b, \quad \rho < a \tag{30}$$

And for superconducting circular microstrip antenna, we have:

$$e_n(\rho) = \int_0^\infty dk_\rho k_\rho \bar{H}_n(k_\rho\rho) \cdot (\bar{G}(k_\rho) - \bar{Z}_S)\bar{K}_n(k_\rho) = \mathbf{0} \qquad \rho < a \tag{31}$$

$$K_n(\rho) = \int_0^\infty dk_\rho k_\rho \bar{H}_n(k_\rho\rho) \cdot \bar{K}_n(k_\rho) = \mathbf{0} \qquad \rho > a \tag{32}$$

Where

$$\bar{Z}_s = \begin{bmatrix} Z_s & 0 \\ 0 & Z_s \end{bmatrix}$$

Galerkin's method is employed to solve the coupled vector integral equations of (29)-(32). Substituting the Hankel transform current expansion of (15) into (29) and (32). Next, multiplying the resulting equation by $\rho\psi_{np}^{+}(\rho)$ (p=1, 2,..... P) and $\rho\varphi_{nq}^{+}(\rho)$ (q=1, 2,..... Q) and using Parseval's theorem for VHT, we obtain a system of Q+ P linear algebraic equations for each mode n which may be written in matrix form. Following well known procedures, we obtain the following system of linear algebraic equations:

$$\begin{bmatrix} \left(\bar{\mathbf{Z}}'^{\Psi\Psi}\right)_{P\times P} & \left(\bar{\mathbf{Z}}'^{\Psi\Phi}\right)_{P\times Q} \\ \left(\bar{\mathbf{Z}}'^{\Phi\Psi}\right)_{Q\times P} & \left(\bar{\mathbf{Z}}'^{\Phi\Phi}\right)_{Q\times Q} \end{bmatrix} \cdot \begin{bmatrix} \left(\mathbf{A}'\right)_{P\times 1} \\ \left(\mathbf{B}'\right)_{Q\times 1} \end{bmatrix} = \mathbf{0} \tag{33}$$

Each element of the submatrices $\bar{\mathbf{Z}}^{CD}$ is given by:

$$\bar{Z}'^{CD}_{ij} = \int_0^\infty dk_\rho k_\rho \mathbf{C}^+_{ni}\left(k_\rho\right) \cdot \left(\bar{G}\left(k_\rho\right) - \bar{Z}_S\right) \cdot \mathbf{D}_{nj}\left(k_\rho\right) \tag{34}$$

Where C and D represent either ψ or φ, for every value of the integer n.

The integration path for the integrals of (32) is, in general, located in the first quadrant of the complex plane k_ϱ. This integration path must remain above the pole and the branch point of $\bar{G}$. Although other choices of branch cut are possible, the choice made in this paper is very convenient, this treated in section 3. Once the impedance and the resistance matrices have been calculated, the resulting system of equations is then solved, for the unknown current modes on the microstrip patch. Nontrivial solutions can exist, if the determinant of Eq. (35) vanishes, that is:

$$\det[\bar{\mathbf{Z}}'(f)] = 0 \tag{35}$$

In general, the roots of this equation are complex numbers indicating, that the structure has complex resonant frequencies ($f = f_r + i f_i$). The bandwidth of a structure operating around its resonant frequency, can be approximately related to its resonant frequency, though the well-known formula ($BW = 2 f_i / f_r$). Once the problem is solved for the resonant frequency, far field radiation, co-polar and cross- polar fields in spherical coordinates are given from.

$$\begin{bmatrix} E_\theta(\bar{r}) \\ E_\varphi(\bar{r}) \end{bmatrix} = \sum_{n=-\infty}^{+\infty} e^{in\varphi}.(-i)^n.e^{ikr}.\bar{T}(\theta)\cdot\bar{V}(k_\rho)\cdot\left(\bar{G}\left(k_\rho\right) - \bar{Z}_S\right)\cdot\bar{K}_n(k_\rho) \tag{36}$$

Where

$$\bar{V}(k_\rho) = \begin{bmatrix} 1 & 0 & -\dfrac{k_\rho}{k_z} \\ 0 & 1 & 0 \end{bmatrix} \text{ and } (\theta) = \begin{bmatrix} \cos\theta & 0 & -\sin\theta \\ 0 & 1 & 0 \end{bmatrix}$$

The losses in the antenna comprise dielectric loss P_d, the conductor loss P_c, and the radiation loss P_r, are given by [4-6]:

$$P_r = (1/4\eta)\iint \left|E_\theta E_\theta^* + E_\varphi E_\varphi^*\right| r^2 \sin\theta\, d\theta\, d\varphi \tag{37}$$

http://dx.doi.org/10.5772/54665

$$P_c = Z_s \iint \left| H_\varphi^2 + H_\rho^2 \right| dS \tag{38}$$

$$P_d = (\omega \varepsilon tg\delta / 2) \iint \left| E_z \right|^2 dV \tag{39}$$

The efficiency of an antenna can be expressed by:

$$efficiency = P_r / (P_r + P_c + P_d) \tag{40}$$

3. Convergence and comparison of numerical results

Computer programs have been written to evaluate the elements of the impedance, resistance matrices, and then solve the matrix equation (35). To enhance the accuracy of the numerical calculation, the integrals of the matrix elements (33) are evaluated numerically along a straight path above the real axis with a height of about $1k_0$ (Figure 2). In this case, the effects of the surface waves are included in the calculation and knowledge of the pole locations is not required, while the length of the integration path is decided upon by the convergence of the numerical results. The time required to compute the integral depends on the length of the integration path. It is found that length of the integration path required reaching numerical convergence at $100k_0$, also Muller's method that involves three initial guesses, is used for root seeking of (35).

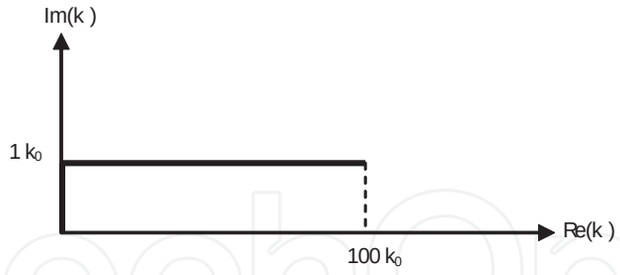

Figure 2. Integration path used for computing the integrals in the complex k_ρ plane

To check the correctness of our computer programs, our results are compared with results of other authors. The comparisons are shown in Table 1 for imperfectly conducting microstrip annular ring antennas. The resonant wave number times the inner radius of the ring is $k_r a$ ($k_r a = 2\pi f_r a\sqrt{\varepsilon_x \varepsilon_0 \mu_0}$), as functions of different sizes of the ratio of the substrate thickness d normalized by the inner radius a is fixed of (0.71cm), and an outer radius of b=2a, the relative permittivity was $\varepsilon_{1z}=\varepsilon_{1x}=2.65$. Annular ring microstrip antenna is excited in the TM_{11} and TM_{12} modes. We found that, for the TM_{11} mode, the real part of ($k_r a$) increases as d/a increases. At the same time, for this mode, the imaginary part of ($k_r a$), which includes the losses by radiation of the

structure, is approximately zero. This means that, the TM_{11} mode has narrow bandwidth and weak-radiation. In addition, we observe that, for the TM_{12} mode, the real part of ($k_r a$) decreases as (d/a) increases, the TM_{12} has relatively wide bandwidth and high-radiation. Therefore, the TM_{11} mode is good for resonator applications and the TM_{12} mode for antennas. It is for that one does the applications of the annular ring microstrip antenna in the TM_{12} mode, better than in the TM_{11} mode. Thus, for this reason, the considered mode in this work is the TM_{12} mode. It is clear from Table 1 that our results agree very well with results obtained by other authors [14, 12].

d/a	Mode TM_{12}						Mode TM_{11}			
	Results of [14]		Results of [12]		Our results		Results of [14]		Our results	
	Re ($k_r a$)	Im ($k_r a$)	Re ($k_r a$)	Im ($k_r a$)	Re ($k_r a$)	Im ($k_r a$)	Re ($k_r a$)	Im ($k_r a$)	Re ($k_r a$)	Im ($k_r a$)
0.005	3.26	0.002	3.24	0.002	3.257	0.002	0.67	$1{,}6.10^{-4}$	0.676	$1{,}6.\ 10^{-4}$
0.01	3.24	0.003	3.23	0.002	3.248	0.003	0.68	$1{,}7.\ 10^{-4}$	0.682	$1{,}8.\ 10^{-4}$
0.05	3.13	0.008	3.10	0.006	3.085	0.006	0.70	$5{,}4.\ 10^{-4}$	0.695	$5{,}5.\ 10^{-4}$
0.1	3.01	0.014	2.96	0.0103	2.968	0.016	0.71	0.0012	0.705	0.0012

Table 1. Calculated ($K_r a$) of annular ring microstrip antennas.

In table 2, we have calculated the resonant frequencies for the modes (TM_{11}, TM_{21}, TM_{31}, and TM_{12}) for perfect conducting circular patch with a radius 7.9375mm, is printed on a substrate of thickness 1.5875mm. These values are compared with theoretical and experimental data, which have been suggested in [10]. Note that the agreement between our computed results, and the theoretical results of [10], is very good.

In our results, we need to consider only the P functions of ψ_{np}, and the Q functions of φ_{nq}. The required basis functions for reaching convergent solutions of complex resonant frequencies, using cavity model basis functions are obtained with (P=5, Q=0).

Mode	Results of [10]		Our results	
	Resonant Frequency (GHz)	Quality factors (Q)	Resonant Frequency (GHz)	Quality factors (Q)
TM_{11}	6.1703	19.105	6.2101	19.001
TM_{12}	17.056	10.324	17.120	10.303
TM_{21}	10.401	19.504	10.438	19.366
TM_{01}	12.275	8.9864	12.296	8.993

Table 2. Comparison of resonant frequencies of the first four modes of a perfect conducting circular patch printed on a dielectric substrate (a=7.9375mm, $\varepsilon_x = \varepsilon_z = 2.65$, d=1.5875 mm).

http://dx.doi.org/10.5772/54665

4. Resonant frequency of superconducting patch antenna

Shown in Figures 3-4, is the dependence of resonant frequency on the thickness t of superconducting patch of the antennas. It is observed that, when the film thickness (t) increases, the resonant frequency increases quickly until, the thickness t reaches the value penetration depth (λ_0). After this value, the increase in the frequency of resonance becomes less significant.

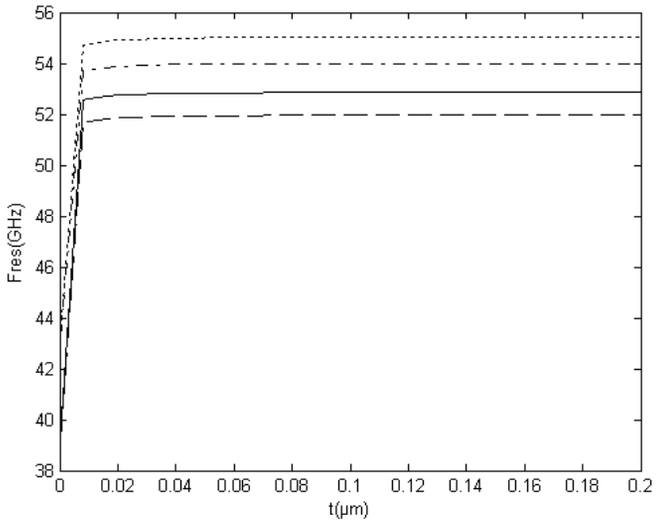

Figure 3. Real part of resonant Frequency against thickness of superconducting annular ring patch antenna. (d=254μm, a=815μm, b=2a, T/ T_C=0.5, λ_0=1500Å, σ_n=210S/mm). (——) ε_x= 9.4, ε_z= 11.6;(– – –) ε_x= 11.6, ε_z= 11.6; (—•—•) ε_x= 13, ε_z=10.3; (……) ε_x=10.3, ε_z= 10.3.

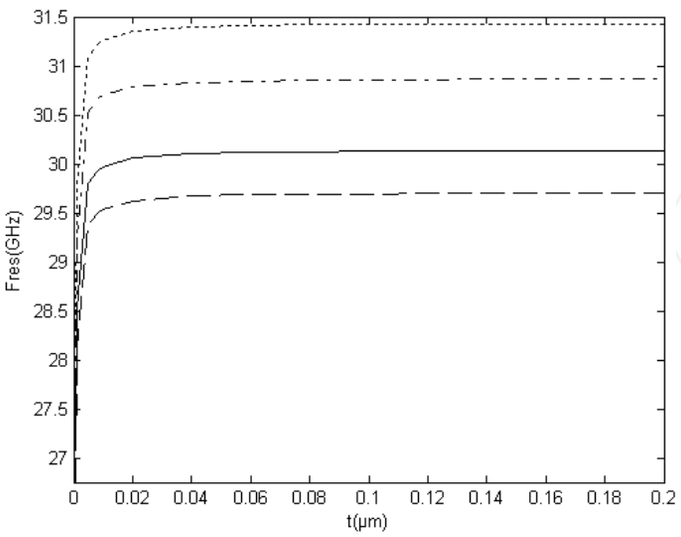

Figure 4. Real part of resonant Frequency against thickness of superconducting circular patch antenna. (d=254μm, a=815μm, T_C =89K, T/ T_C=0.5, λ_0=1500Å, σ_n=210S/mm).(——) ε_x= 9.4, ε_z= 11.6;(– – –) ε_x= 11.6, ε_z= 11.6; (—•—•) ε_x= 13, ε_z=10.3; (……) ε_x=10.3, ε_z= 10.3.

Figures 5-6 demonstrated relations between the real part of frequency resonance, and the normalized temperature (T/Tc), where the critical temperature used here for our data (89K). The variations of the real part of frequency due to the uniaxial anisotropy decrease gradually with the increase in the temperature. This reduction becomes more significant for the values of temperature close to the critical temperature. These behaviours agree very well with those reported by Mr. A. Richard for the case of rectangular microstrip antennas [2].

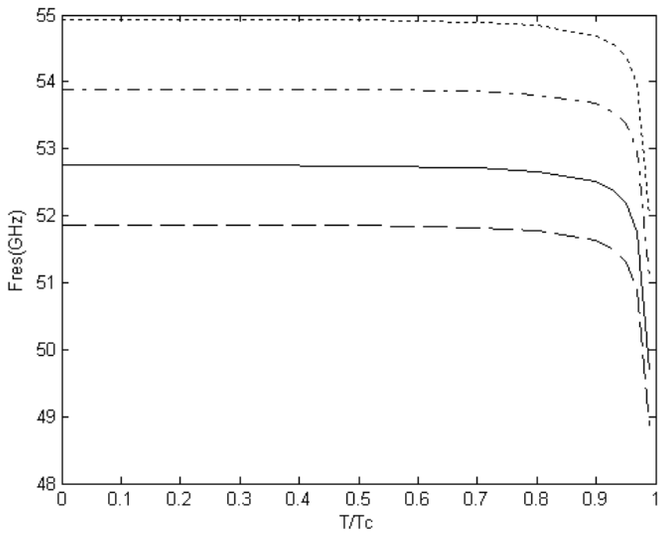

Figure 5. Real part of resonant frequency of superconducting annular ring patch antenna against T/T_C (d=254μm, a=815μm, b=2a, t=0.02μm, λ_0=1500Å, σ_n=210S/mm). (———) ε_x= 9.4, ε_z= 11.6;(– – –) ε_x= 11.6, ε_z= 11.6; (—•—•) ε_x= 13, ε_z=10.3; (……) ε_x=10.3, ε_z= 10.3.

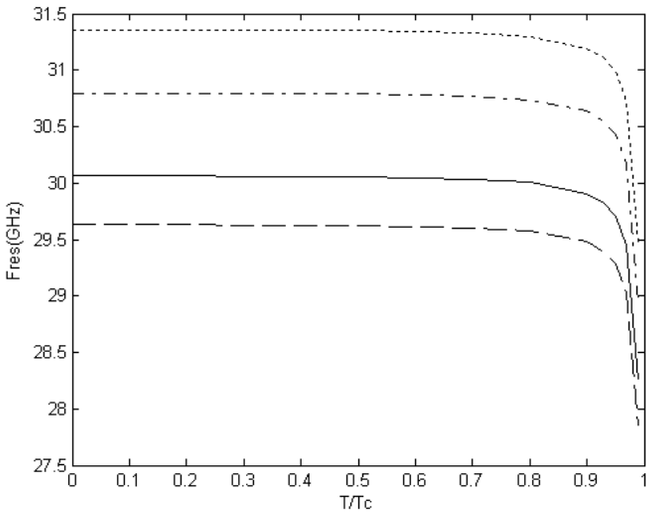

Figure 6. Real part of resonant frequency of superconducting circular patch antenna against T/T_C (d=254μm, a=815μm, T_C =89K, h= 0.02μm, λ_0=1500Å, σ_n=210S/mm). (———) ε_x= 9.4, ε_z= 11.6;(– – –) ε_x= 11.6, ε_z= 11.6; (—•—•) ε_x= 13, ε_z=10.3; (……) ε_x=10.3, ε_z= 10.3.

http://dx.doi.org/10.5772/54665

5. Radiations patterns and efficiency of superconducting patch antenna

The calculated radiations patterns (electric field components, Eθ; E_{φ}), of the microstrip antenna on a finite ground plane in the E plane, and in the H plane are plotted in Figs. 7 -10, printed on an uniaxial anisotropy substrate thickness (d=254μm). The mode excited for superconducting annular ring patch antenna is the TM_{12} and for superconducting circular patch antenna is the TM_{11}. It is seen that the permittivity ε_z has a stronger effect on the radiation than the permittivity ε_x. The radiation pattern of an antenna becomes more directional as its ε_z increases. Another useful parameter describing the performance of an antenna is the gain. Although the gain of the antenna is related to the directivity, the gain of an antenna becomes high as its ε_z increases.

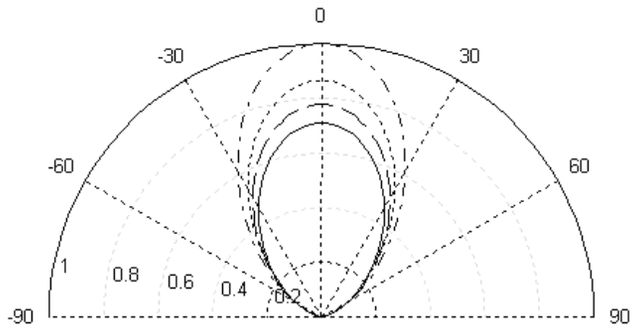

Figure 7. Radiation pattern versus angle θ of superconducting annular ring patch antenna at φ=0° plane (a=815μm, b=2a, t=0.02μm,d=254μm, λ0=1500Å, σ_n=210S/mm). (——)ε_x= 9.4, ε_z= 11.6; (– – –)ε_x= 11.6, ε_z= 11.6;(— • — •) ε_x= 13, ε_z=10.3 ;(……) ε_x=10.3, ε_z= 10.3.

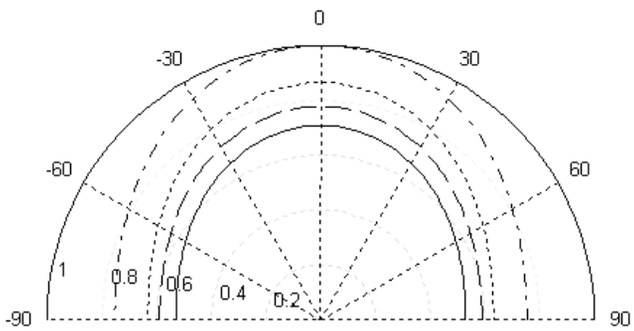

Figure 8. Radiation pattern versus angle θ of superconducting annular ring patch antenna at φ=90° plane (a=815μm, b=2a, t=0.02μm, d=254μm, λ0=1500Å, σ_n=210S/mm).(——)ε_x= 9.4, ε_z= 11.6;(– – –)ε_x= 11.6, ε_z= 11.6; (— • — •) ε_x= 13, ε_z=10.3 ; (……) ε_x=10.3, ε_z= 10.3.

In calculation of losses, we have found that, the values of dielectric loss (P_d), the conductor loss (P_c), and the radiation loss (P_r) will depend on frequency. We use results precedents to calculate the variation of radiation efficiency as a function of resonant frequency, for various isotropic dielectric substrates. Our results are shown in Figs. 11 and 12. It is seen that the efficiency increases with decreasing frequencies. The same behaviour is found by R. C. Hansen [1].

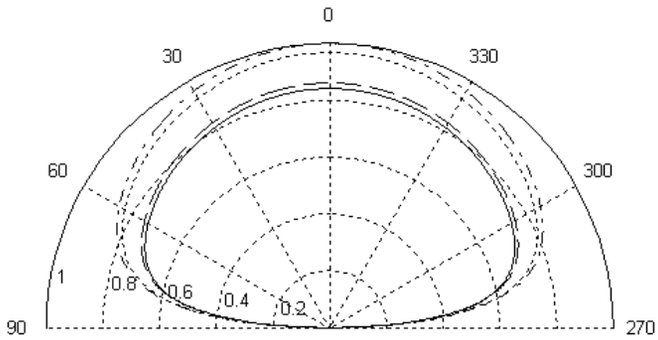

Figure 9. Radiation pattern versus angle θ of superconducting circular patch antenna at φ=0° plane (a=815μm, t=0.02μm, T/ T_C=0.5, d=254μm, λ_0=1500Å, $_n$=210S/mm). (——) ε_x= 9.4, ε_z= 11.6; (– – –) ε_x= 11.6, ε_z= 11.6; (— • — •) ε_x= 13, ε_z=10.3 ; (……) ε_x=10.3, ε_z= 10.3.

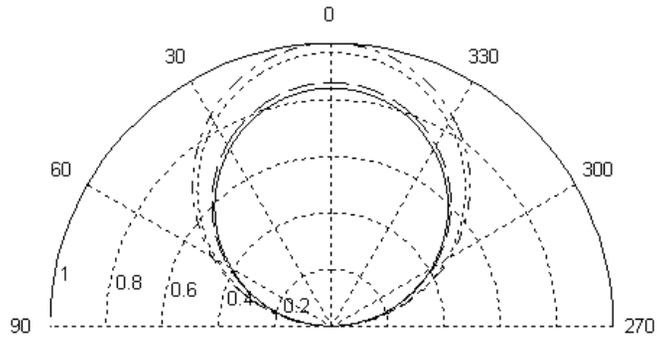

Figure 10. Radiation pattern versus angle θ of superconducting circular patch antenna at φ=π/2 plane (a=815μm, h=0.02μm, T/ T_C=0.5, d=254μm, λ_0=1500Å, $_n$=210S/mm). (——) ε_x= 9.4, ε_z= 11.6; (– – –) ε_x= 11.6, ε_z= 11.6; (— • — •) ε_x= 13, ε_z=10.3 ; (……) ε_x=10.3, ε_z= 10.3.

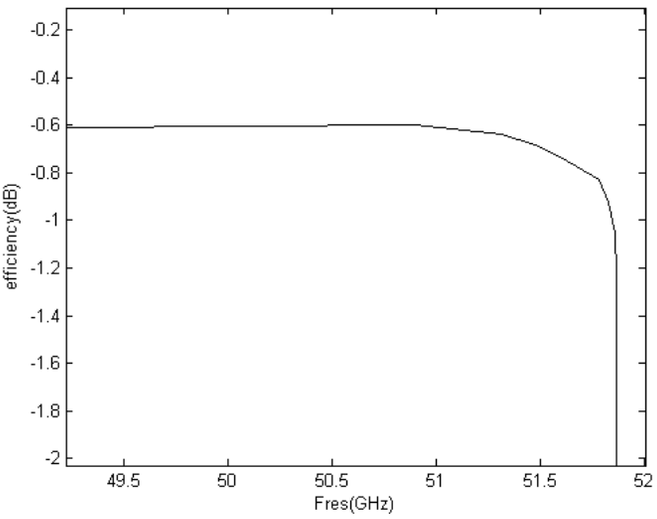

Figure 11. Superconducting annular ring patch antenna efficiency for the mode TM_{12} (d=254μm, a=815μm, b=2a, t=0.02μm, λ_0=1500Å, σ_n=210S/mm, ε_x= ε_z=11.6, δ=0.0004).

http://dx.doi.org/10.5772/54665

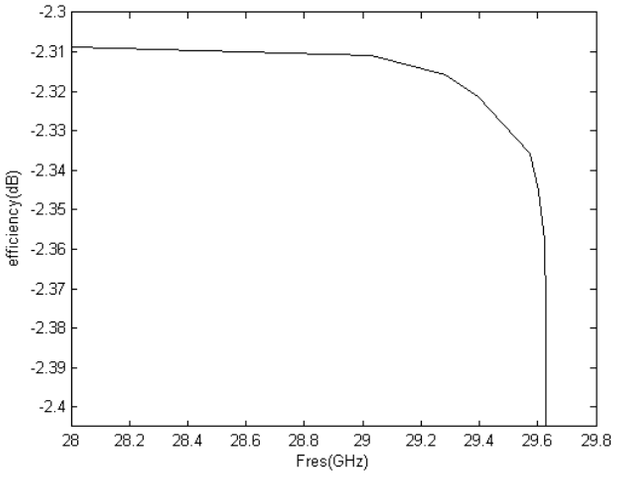

Figure 12. Superconducting circular patch antenna efficiency for the mode TM_{11} ((d=254μm, a=815μm,h=0.02μm, T/T_C=0.5, λ_0=1500Å, σ_n=210S/mm, $\varepsilon_x = \varepsilon_z$=11.6, δ=0.0024).

6. Conclusion

This work presents a fullwave analysis for the superconducting microstrip antenna on uniaxial anisotropic media. The complex resonant frequency problem of structure is formulated in terms of an integral equation. Galerkin procedure is used in the resolution of the electric field integral equation, also the TM, TE waves are naturally separated in the Green's function. In order to introduce the effect of a superconductor microstrip patch, the surface complex impedance has been considered. Results show that the superconductor patch thickness and the temperature have significant effect on the resonant frequency of the antenna. The effects of a uniaxial substrate on the resonant frequency and radiation pattern of structures are considered in detail. It was found that the use of such substrates significantly affects the characterization of the microstrip antennas, and the permittivity (ε_z) along the optical axis has a stronger effect on the radiation of antenna. Thus, microstrip superconducting could give high efficiency with high gain in millimeter wavelengths. A comparative study between our results and those available in the literature shows a very good agreement.

Author details

Ouarda Barkat*

Electronics Department, University of Constantine, Constantine, Algeria

References

[1] Hansen, C R. Electrically Small, Superdirective, and Superconducting Antennas. John Wiley& Sons, Inc, Hoboken, New Jersey, (2006).

[2] Richard, M A. Bhasin B K & Clapsy C P. Superconducting microstrip antennas: an experimental comparison of two feeding methods. *IEEE Transactions on Antennas Propagation,* AP-(1993). , 41, 967-974.

[3] Barkat, O, & Benghalia, A. Radiation and resonant frequency of superconducting annular ring microstrip antenna on uniaxial anisotropic media. *Springer, Journal of Infrared, Millimeter, and Terahertz Waves,* (2009). , 30(10)

[4] Garg, R, & Bhartia, P. Bahl, & Ittipiboon A I. *Microstrip Antenna Design Handbook.* Artech House, Boston, London, (2001).

[5] Lee F H & Chen W*Advances in microstrip and printed antennas.* New York, John Wiley & Sons, (1997).

[6] James, R J, & Hall, P S. *Handbook of Microstrip Antennas.* Peter Peregrinus Ltd, London, (1989).

[7] Yang, M G, Xing, X, Daigle, A, Obi, O, Liu, M, Lou, J, Stoute, S, Naishadham, K, & Sun, N X. Planar Annular Ring Antennas With Multilayer Self-Biased NiCo-Ferrite Films Loading. *IEEE Transactions on antennas and propagation*., (2010). , 58(3)

[8] Richard, M A, Bhasin, K B, & Claspy, P C. Performance of a K-band superconducting annular ring antenna. *microwave and optical technology letters*., (1992). , 5(6)

[9] Gürel, S Ç, & Yazgan, E. Modified cavity model to determine resonant frequency of tunable microstrip ring antennas. *Taylor and Francis, Electromagnetic,191999*, 443-455.

[10] Losada, V. BOIX R R & Horno M. Resonant modes of circular microstrip patches in multilayered substrates, IEEE Transactions on Microwave Theory and techniques (1999). , 47, 488-497.

[11] Chew W C & Kong J AResonance of non axial symmetric modes in circular micro strip disk. *J. Math. Phys.* (1980). , 21(10)

[12] [12]Ali, S M, Chew, W C, & Kong, J A. Vector Hankel transform analysis of annular ring microstrip antenna. *IEEE Transactions on Antennas and Propagation*, July (1982). , AP-30(4)

[13] Cai Z & Bornemann JGeneralized Spectral Domain Analysis for Multilayered Complex Media and High Tc Superconductor Application. *IEEE Transactions on microwave Theory and Techniques*, (1992). , 40(12)

[14] Chew, W C. A broad band annular ring microstrip antenna. *IEEE Transactions on Antennas and Propagation*. (1982). , AP-30